Polymer 230 (2021) 124041

Contents lists available at ScienceDirect

Polymer

journal homepage: www.elsevier.com/locate/polymer

Luminescent molecularly imprinted polymer nanocomposites for emission intensity and lifetime rapid sensing of tenuazonic acid mycotoxin

José Quílez-Alburquerque [a], Ana B. Descalzo [a,**], María C. Moreno-Bondi [b], Guillermo Orellana [a,*]

[a] Department of Organic Chemistry, Faculty of Chemistry, Complutense University of Madrid (UCM), 28040, Madrid, Spain
[b] Department of Analytical Chemistry, Faculty of Chemistry, Complutense University of Madrid (UCM), 28040, Madrid, Spain

ARTICLE INFO

Keywords:
Luminescence
Molecularly imprinted polymers
Nanoparticles
Ruthenium(II) complexes
Tenuazonic acid

ABSTRACT

Tenuazonic acid ((5*S*)-3-acetyl-5-[(2*S*)-butan-2-yl]-4-hydroxy-2,5-dihydro-1*H*-pyrrol-2-one, TeA) is a widespread *Alternaria* fungi mycotoxin in food produce. This toxin may be allergenic and provoke hay fever and asthma. Therefore, rapid methods to selectively detect TeA are needed. With this aim, we have engineered a novel trifunctional (red-luminescent, polymerizable, TeA-sensitive) ruthenium(II)-bipyridyl complex with 2,2′-biimidazole. Its peripheral N–H moieties recognize the enolate form of 1,3-dicarbonyl compounds (including TeA) in partially aqueous media. Such a binding decreases the luminescence intensity and lifetime (0.2 μs) of the Ru(II) probe. The probe also bears acrylate groups that allow radical copolymerization with methacrylamide and ethylene glycol dimethacrylate in the presence of TeA, to yield 9-nm thick luminescent molecularly imprinted polymer (MIP) shells onto 200-nm silica cores. The SiO_2@Ru-MIP nanocomposite displays a very fast response (<5 s) suitable for real-time detection of TeA. No cross-sensitivity to other common food mycotoxins that also contain a β-hydroxycarbonyl moiety (alternariol, β-zeranol, cyclopiazonic acid) is observed. Detection limits of 63.8 μg L^{-1} and 75.2 μg L^{-1} under steady-state and time-resolved luminescence detection, respectively, have been measured without further optimization. The use of emission lifetime variations to monitor the levels of a target analyte has never been reported for a luminescent MIP-based sensor.

1. Introduction

Tenuazonic acid, (5*S*)-3-acetyl-5-[(2*S*)-butan-2-yl]-4-hydroxy-2,5-dihydro-1*H*-pyrrol-2-one or TeA (Scheme 1a), is a widespread mycotoxin produced mainly by *Alternaria* fungi that grow on vegetables, oilseeds, fruits and cereal grains among other foods [1,2]. This ubiquitous species is often allergenic to humans, grow indoors and may cause hay fever or hypersensitivity reactions leading to asthma. In addition to TeA, *Alternaria* fungi produce other toxic secondary metabolites such as alternariol (AOH), alternariol monomethyl ether and altenuene [3]. TeA is the most toxic chemical of the family (e.g. LD_{50} 81–186 mg kg^{-1} body weight for mice, 168–180 mg kg^{-1} b.w. for rats, and 0.55 mg per egg for chicken embryos) [4]. Different studies have confirmed the co-occurrence of *Alternaria* toxins in high levels, from μg kg^{-1} to mg kg^{-1}, in food [5,6]. No guideline limits for TeA in foods have been set so far by the regulatory authorities, despite this mycotoxin has been identified as toxicologically relevant for public safety [7].

Several methods for TeA quantification have been described. The simplest ones are those based on high performance liquid chromatography (HPLC) with UV absorption detection. Nevertheless, due to the faint absorption of TeA in this region, they display low detectability and reproducibility that are improved by addition of $ZnSO_4$ to the mobile phase to carry out metal complexation with the analyte [8]. Much more sensitive HPLC-mass spectrometry (MS) methods with double or even triple mass detector have been developed [9–11]; however, in addition to the cost of the instrumentation, they often require previous clean-up and preconcentration steps using solid phase extraction [10] or the so called 'QuEChERS' [11]. Therefore, the development of sensitive, selective, straightforward analytical methods for rapid inexpensive quantification of TeA, applicable to in situ determinations, is highly desirable.

Luminescence is arguably one of the best choices to develop novel

* Corresponding author.
** Corresponding author.
E-mail addresses: ab.descalzo@quim.ucm.es (A.B. Descalzo), orellana@quim.ucm.es, guillermo3ono@gmail.com (G. Orellana).

https://doi.org/10.1016/j.polymer.2021.124041
Received 4 June 2021; Received in revised form 15 July 2021; Accepted 20 July 2021
Available online 2 August 2021

chemosensing platforms, thanks to its high sensitivity, good selectivity, versatility (intensity, lifetime and polarization measurements are possible), and long-term stability (if ratiometric-intensity or emission lifetime-based measurements are used) [12,13]. In this regard, we have devoted significant efforts to the molecular tailoring, preparation and photochemical characterization of red-luminescent polypyridyl ruthenium(II) complexes for industrial, environmental and clinical sensing [14]. These dyes show unique properties such as high (photo)chemical stability, long emission lifetimes (up to 7 μs), large Stokes shifts (>150 nm), and luminescence quantum yields between 0.4 and 0.04. Furthermore, their photochemical properties and polymer-supporting method may be finely tuned to the target analyte by a judicious selection of the ligands.

In order to recognize the target species, at least an analyte-selective ligand must be introduced in the Ru(II) complex coordination sphere. TeA displays keto-enol tautomerism because of its triple β-dicarbonyl structure (Scheme 1a, pK_a = 3.5) [15]. Considering the chemical structure and properties of TeA, we propose the 2,2′-biimidazole (bim) ligand as a suitable receptor. Its double bidentate feature allows incorporation to the metal coordination sphere while keeping its role as receptor of bidentate anions of adequate geometry by establishing two simultaneous hydrogen bonds (Scheme 1b) [16]. Several studies confirm the use of transition metal-bim complexes as luminescent probes for optical transduction upon molecular recognition [17], but their interaction with 1,3-diketonate anions has not been investigated so far. The use of Ru(II)-bim complexes as probes of β-diketonates may be of interest not just in the analysis of food contaminants (the above-mentioned TeA, the related cyclopiazonic acid, or the β-zearalenone and zeranol mycotoxins) [18], but also in other fields such as sensing of fluoroquinolone antibiotics [19] and sensitizers for photodynamic therapy (PDT) like curcumin and curcuminoids [20].

The probe selectivity towards TeA can be further improved through combination of the luminescent features of Ru(II) complexes with a molecularly imprinted polymer (MIP) as recognition element. MIPs are biomimetic materials synthesized in the presence of a template molecule, normally the target analyte or a structural surrogate of it, by copolymerization of complementary functional monomers and a cross-linker [21,22]. The template is removed after the polymerization, leaving behind empty cavities into a highly cross-linked matrix which are complementary in size, shape, and functional groups to the template. The MIPs long-term stability, high selectivity, low cost and robustness [23], have led to their success in different applications such as sensors [24,25], enzyme mimicking and catalysis [26], and solid-phase extraction [27]. Regarding their application to chemical sensing, one of the main handicaps of using MIPs is their highly crossed-linked nature. While required to provide rigidity to the binding cavity, it yields slow analyte diffusion rates. A way to circumvent this problem is to increase the surface-to-volume ratio of the MIP materials, so that mass-transfer processes speed up. The latter can be achieved, for example, by using core-shell nanoparticles where the MIP is grown as a few-nm layer onto a non-imprinted core substrate such as a silica, quantum dot, or carbon dot nanoparticle [28–30]. Furthermore, the template is efficiently removed, an issue of utmost importance for the analysis of trace levels [31].

Incorporation of a luminescent probe in the MIP backbone allows detection of the target analyte if binding to the latter changes the probe emission features. Intensity-based luminescence measurements are very sensitive and straightforward to use. However, they may display poor reproducibility for particulate materials due to light scattering, probe photobleaching or excitation light source drift. These drawbacks are suppressed if the probe luminescence lifetime as a function of the analyte concentration is monitored instead [32].

In this paper we describe a luminescent MIP based on a tailored multifunctional Ru(II) complex containing a biimidazole ligand as the β-diketonate recognition moiety. The polymerizable probe belongs to the MIP scaffold, grown as a nanolayer onto SiO_2 nanobeads for tenuazonic acid sensing. Fast diffusion of the analyte through the few nm-thick MIP shell provides a selective instantaneous optical response. The system allows detection of ng mL^{-1} amounts of TeA in partially aqueous media by measuring changes in either the luminescence intensity or lifetime of the Ru(II)-doped material.

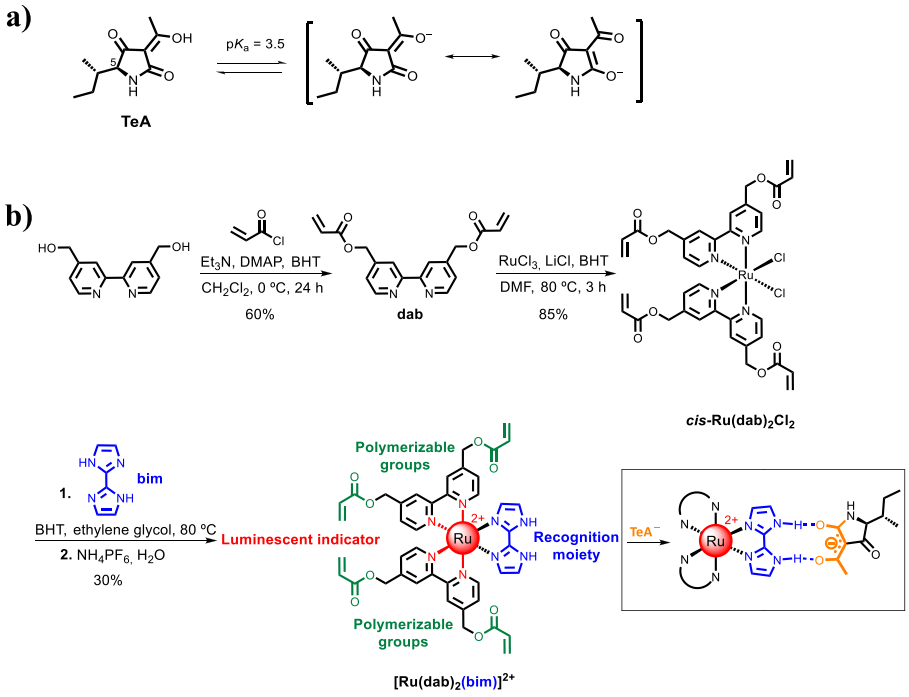

Scheme 1. a) Structure of the most abundant tautomer of Tenuazonic acid (TeA) mycotoxin in aqueous solution. b) Synthesis of the trifunctional $[Ru(dab)_2(bim)]^{2+}$ monomer-probe in three steps, and proposed interaction of the latter with the diketonate form of tenuazonic acid (TeA^-).

2. Experimental

2.1. Materials

The precursor 2,2′-biimidazole (bim) and 2,2′-bipyridin-4,4′-diyldimethyl diacrylate (dab) ligands were synthesized by literature procedures [33,34]. The intermediate *cis*-[Ru(dab)$_2$Cl$_2$] complex was prepared by adapting a general method (see below) [35]. All reactions involving Ru(II) were carried out under argon. The 'synthetic' tenuazonic acid, a mixture of the 5*S* and 5*R* (81:19) diastereoisomers (as per HPLC analysis of the diastereoisomers mixture), was obtained from L-isoleucine methyl ester by a reported procedure [36].

Lithium chloride and Ru(III) chloride trihydrate, were purchased from Acros Organics (Belgium). Butylhydroxytoluene (BHT), acryloyl chloride, tetrabutylammonium hydroxide, tetrabutylammonium fluoride, ethyleneglycol dimethacrylate (EDMA), tetraethyl orthosilicate (TEOS), carbon disulfide, and phenylmagnesium bromide (1 M solution in THF) were from Merck (Germany). 4,4′-Bis(hydroxymethyl)-2,2′-bipyridine was from TCI (Japan), whereas tetrabutylammonium acetate and 4-(chloromethyl)phenyltrichlorosilane were from Alfa Aesar (Germany). Methacrylamide (MAM) was supplied by Fluka (Switzerland). Ammonium hexafluorophosphate was from Fluorochem (UK). The initiator *N,N*-azobis(2,4-dimethyl)valeronitrile (ABDV) was purchased from Wako (Germany) and used as received. Alternariol (AOH) was from Apollo Scientific (UK), while cyclopiazonic acid (CPA) and β-zeranol (β-ZOL) were from Merck. The natural TeA was isolated from the commercial Cu(II) bis-chelate complex (Cayman Chemical, USA; +98%) by dissolving the complex in methylene chloride and slowly passing it through a column containing Dowex 50X8 resin. *m*-Xylene, anhydrous dimethylformamide (DMF) and anhydrous tetrahydrofuran (THF) were from Merck, whereas toluene, methanol (MeOH) and acetonitrile (MeCN) (all HiPerSolv Chromanorm HPLC grade) were from VWR (Germany). Trifluoroacetic acid (99%) was from Fluorochem, hydrochloric acid (37%) was from Fisher Scientific (UK), and ethylene glycol (+99%) from Scharlau (Spain). Type I ultrapure water was produced with a Merck Millipore (US) Direct-Q-3UV system. Deuterated solvents with tetramethylsilane (TMS) as internal reference were from VWR.

2.2. Instrumentation

UV–vis absorption spectra were recorded with a Varian Cary 3-Bio spectrophotometer (CA, USA). Steady-state luminescence spectra of the indicator dyes in solution were measured with either a FluoroSENS (Gilden Photonics, UK) or a Horiba (Japan) Fluoromax-4TCSPC spectrofluorometer, both fitted with a red-sensitive R928 photomultiplier (Hamamatsu, Japan; response up to 850 nm) and equipped with a 150 W xenon lamp. The excitation wavelength was always set at 500 nm and the luminescence spectra have been corrected for the instrument response in all cases. Luminescence lifetime measurements were performed on an Edinburgh Instruments (UK) FLS980-Xd2-T spectrometer equipped with a Horiba 470LH diode laser (463 nm, <1 ns pulse width), an excitation 467-nm bandpass interference filter, a 500 nm-blazed double monochromator in the emission channel, and a Hamamatsu R928P photomultiplier thermoelectrically cooled at −21 °C.

2.3. Synthesis of cis-Ru(dab)$_2$Cl$_2$

143 mg (0.69 mmol) of ruthenium(III) chloride hydrate, 450 mg (1.39 mmol) of dab, 118 mg (2.77 mmol) of lithium chloride and 2 mg of BHT (9.07 x 10^{-3} mmol) were dissolved in 3 mL of anhydrous DMF. The solution was kept at 80 °C for 2 h under argon with stirring. When TLC in silica (MeCN–water–KNO_3 satd. aq. soln. 50:2:1 v/v/v) showed a complete consumption of the starting materials, the reaction mixture was cooled down and the dichloro Ru(II) complex was precipitated by slow addition of a mixture of dichloromethane and diethyl ether (1:1 v/v). The resulting deep purple solid was collected by filtration and dried overnight in a vacuum oven (30 °C, 0.01 Torr; 85% yield). UV–vis (MeCN): λ_{max} (ε/M^{-1}cm^{-1}) 498 (2950), 380 (4550), 300 nm (19200).

2.4. Synthesis of [Ru(dab)$_2$(bim)]$^{2+}$

650 mg (0.79 mmol) of *cis*-Ru(dab)$_2$Cl$_2$, 108 mg (0.79 mmol) of 2,2′-biimidazole and 2 mg of BHT (9.07 x 10^{-3} mmol) were dissolved in 4 mL of ethylene glycol. The solution was kept at 80 °C for 1 h under argon until the TLC (silica; MeCN–water–KNO_3 satd. soln. 50:2:1 v/v/v) showed complete consumption of the starting materials. Then, the reaction mixture was cooled and 2 mL of water was added. The heteroleptic complex precipitated upon addition of a saturated aqueous solution of ammonium hexafluorophosphate and was collected and washed with water. The resulting solid was purified by column chromatography (silica gel; methylene chloride–methanol 9:1 v/v) to afford a deep red product in 30% yield. ^{1}H NMR (300 MHz, CD_3CN, TMS) δ: 8.41 (s, 4H), 7.91 (d, $J = 6$ Hz; 2H), 7.81 (d, $J = 6$ Hz; 2H), 7.41 (d, $J = 5$ Hz; 2H), 7.30 (d, $J = 5$ Hz; 2H), 7.21 (s, 2H), 6.44 (m, 4H), 6.30 (m, 6H), 5.99 (m, 4H), 5.37 (s, 4H), 5.33 ppm (s, 4H). ^{13}C NMR (500 MHz, CD_3CN, TMS) δ: 164.2, 164.1, 162.5, 161.7, 159.7, 158.7, 154.0, 153.5, 142.8, 142.7, 141.7, 135.5, 135.4, 128.8, 126.46, 125.8, 122.3, 122.1, 122.0, 116.28, 43.22 ppm. MS (ESI) *m/z*: [M$^+$ − H] calcd. for $C_{42}H_{37}N_8O_8Ru$, 883.2; found, 883.3. UV–vis (MeCN): λ_{max} (ε/M^{-1}cm^{-1}) 485 (8448), 346 (10570), 292 nm (56932).

2.5. Preparation of the RAFT agent-bonded SiO$_2$ particles

200-nm dia. SiO_2 nanobeads were obtained by a modified Stöber method [37]. Briefly, TEOS (8.0 mL) was quickly added to a solution of ethanol (800 mL), water (200 mL) and 32% ammonia aq. solution (54 mL). The reaction mixture was kept for 24 h at room temperature under stirring (300 rpm). The nanobeads were isolated by centrifugation (11,000 rpm), washed with 20 mL of ethanol (3x), and resuspended in ethanol (54 mg mL^{-1}).

Before modifying the Stöber nanoparticles surface, an activation/rehydroxylation step is needed. To achieve it, the ethanol was removed, and the nanoparticles were washed with 20 mL of water and resuspended in 30 mL of water. Then, 7.5 mL of 37% HCl was added, and the mixture was kept under reflux for 5 h. The reaction mixture was cooled down to room temperature and the particles were washed by centrifugation (11,000 rpm) with ca. 20 mL of water (3x), 20 mL of MeOH (3x) and 20 mL of toluene (2x), and resuspended in toluene. After activation of the nanobeads surface, the silanization procedure follows. 4-(Chloromethyl)phenyltrichlorosilane (3.0 mL) was added to 40 mL of an argon-sparged anhydrous toluene suspension of ca. 2 g of activated beads placed in a two-neck round-bottom flask. Then, a solution of triethylamine (1.86 mL) in dry toluene (10 mL) was incorporated dropwise, and the reaction mixture refluxed overnight under argon. Finally, the silanized nanoparticles were washed by centrifugation with toluene (3x), MeOH (3x) and THF (3x), using *ca.* 20 mL for each washing.

To covalently attach the RAFT agent, carbon disulfide (4.6 mL) was added dropwise to a solution of phenylmagnesium bromide (30 mL; 1.0 mol L^{-1} in THF), previously sparged with argon for 15 min, to give a deep red solution. The reaction mixture was stirred at 50 °C for 1 h. Then, ca. 2 g of silane-modified SiO_2 nanobeads suspended in 40 mL of dry THF was added, and the mixture was stirred at 50 °C for 3 h. Finally, the functionalized particles were washed by centrifugation with THF (3x) and MeCN (3x), using ca. 20 mL for each washing.

2.6. Preparation of SiO$_2$@Ru-MIP nanobeads

Synthetic tenuazonic acid (TeA, 1.0 mg; 0.005 mmol), tetrabutylammonium hydroxide solution in dry MeOH (5 μL; 5 μmol), and [Ru(dab)$_2$(bim)]$^{2+}$ monomer (6.0 mg; 5 μmol) were combined in 5 mL of MeCN. The mixture was cooled at 8 °C for 1 h to favor interactions

between the functional monomer and the template molecule. Then, MAM (9.4 mg, 0.11 mmol), EDMA (90 μL, 0.47 mmol), and ABDV (5 mg, 0.02 mmol) were added, plus a suspension of 7.5 mg of RAFT agent-functionalized SiO_2 beads in 5 mL of MeCN. The mixture was sparged with argon and kept at 70 °C for 24 h. For removing the template (TeA), the beads were washed with a MeOH–TFA mixture (9:1 v/v) (3 x 15 mL) and then with acetonitrile (3 x 15 mL). The non-imprinted polymer (NIP) particles were synthesized under the same conditions but without adding the template molecule.

3. Results and discussion

3.1. Synthesis of the $[Ru(dab)_2(bim)]^{2+}$ trifunctional monomer

Scheme 1b depicts the chemical structure and procedure to prepare the luminescent $[Ru(dab)_2(bim)]^{2+}$ dye containing four polymerizable acryloyl groups in two dab ligands to allow its covalent incorporation into the MIP matrix, and the bim ligand for recognizing TeA. The dab ligand was readily synthesized in 60% yield from commercial bipyridine-4,4′-dimethanol and acryloyl chloride [34]. The *cis*-$Ru(dab)_2Cl_2$ precursor was prepared by adapting a general procedure to synthesize *cis*-$Ru(bpy)_2Cl_2$ [35], in which the stoichiometric amount of dab was mixed with $RuCl_3$ in the presence of a small amount of butylhydroxytoluene (BHT) to inhibit the untimely radical polymerization, and a large excess of LiCl to prevent formation of the tris-dab complex. The target Ru(II) probe was synthesized by reacting *cis*-$Ru(dab)_2Cl_2$ and 2,2′-biimidazole (bim) in hot ethylene glycol for solubility reasons. The trifunctional metal complex was isolated by precipitation as its PF_6^- salt. Fig. S1–S4 show the NMR, MS and FTIR data that confirm the identity of the $[Ru(dab)_2(bim)](PF_6)_2$ complex.

3.2. Spectroscopic characterization of the $[Ru(dab)_2(bim)]^{2+}$ luminescent probe

Ru(II) complexes containing the 2,2′-biimidazole ligand have already been described as receptors for simple anions such as bromide, fluoride, phosphate or acetate based on hydrogen bonding interactions, but not for β-dicarbonyl compounds [17]. These studies show that their absorption, emission and redox properties depend on the protonation state of this ligand, as it includes two peripheral N–H moieties that may undergo double deprotonation with strong bases such as fluoride in organic media [38,39]. For acetate detection, Cui et al. employed luminescent $[Ru(bpy)_2(bim)]^{2+}$ (bpy stands for 2,2′-bipyridine) in neat acetonitrile and observed a 32-nm red shift of the absorption of the free complex at 475 nm upon addition of AcO^-, with an isosbestic point at 486 nm, and significant quenching of the probe emission (that moved from 635 to 648 nm) [40].

In the case of our $[Ru(dab)_2(bim)]^{2+}$ complex, addition of acetate leads to similar effects. Figs. S5a–b shows that addition of increasing amounts of acetate (as its tetrabutylammonium or "TBA" salt) in neat acetonitrile induces a red shift of the $[Ru(dab)_2(bim)]^{2+}$ probe absorption from 485 nm to 524 nm, with isosbestic points at 413 and 503 nm. When the same study was performed with the target anion, namely the TBA salt of the synthetic TeA (Fig. 1a), very similar changes of the absorption profile were observed: the absorption band of the Ru(II) probe at 485 nm decreases gradually while a new peak at 524 nm appears upon the TeA^- addition, with isosbestic points at 412 nm and 500 nm. The clear isosbestic points obtained are indicative of a defined 1:1 stoichiometry for the $[Ru(dab)_2(bim)]^{2+}$–TeA^- adduct. The titrations displayed in Fig. S5a and Fig. 1a have been employed to determine the binding constants (K_b) of the Ru(II) complex to AcO^- and TeA^- with the HypSpec software (v1.1.50, Protonic Software, www.hyperquad.co.uk) [41]. The best fit of the experimental spectroscopic titration data yields log $K_b(AcO^-)$ = (6.08 ± 0.01) and log $K_b(TeA^-)$ = (6.83 ± 0.03). These results evidence a stronger interaction between the Ru(II)-bim probe and the deprotonated 1,3-dicarbonyl toxin than that with the acetate anion in the same organic medium. This result suggests a more efficient hydrogen bonding of the biimidazole ligand to the 1,3-diketonate anion.

Upon excitation at the 500 nm isosbestic point (Fig. 1b), the free $[Ru(dab)_2(bim)]^{2+}$ shows luminescence at 700 nm in acetonitrile. The emission is dramatically quenched upon addition of either AcO^- or TeA^- (Fig. S5b and Fig. 1b, respectively), with progressive band broadening. The latter suggests the existence of distinct emissive species that result from the interaction via hydrogen bonding and deprotonation of the Ru(II) complex. Favorable electrostatic interactions between $RuL_2(bim)^{2+}$ and TeA^- or AcO^- also contribute to the probe association to these species in acetonitrile.

The emission quenching and band broadening of the $[Ru(dab)_2(bim)]^{2+}$ indicator dye is also observed in acetonitrile solutions upon addition of small amounts of water (Figs. S5c–d). As it is expected for a recognition system relying on hydrogen bonding interactions, an increase of the water content from 0 to 10% in acetonitrile leads to significant changes of the probe luminescence, since water is a strong hydrogen bond donor and acceptor. Water efficiently solvates $[Ru(dab)_2(bim)]^{2+}$ and provokes its (partial) deprotonation, similarly to the effect of bases such as AcO^- (Figs. S5a–b) and TeA^- (Fig. 1a and b), yielding different emissive species. In order to confirm deprotonation of the bim complex, a test with fluoride (a well-known strong base in organic media) in dimethyl sulfoxide solution was carried out (Fig. S6). Upon addition of a 10-fold excess of F^-, the observed 50-nm blue shift of the $[Ru(dab)_2(bim)]^{2+}$ emission confirms its deprotonation. Nevertheless, this hypsochromic shift of the luminescence is not paralleled by the expected blue-shift of the probe absorption (Fig. S6). This is not without precedent for Ru(II) heteroleptic complexes: due to the combined solvent reorientation and geometry relaxation that occur after intersystem crossing to their luminescent ^{3}MLCT triplet state, an increase of the downwards transition energy upon deprotonation may occur [42].

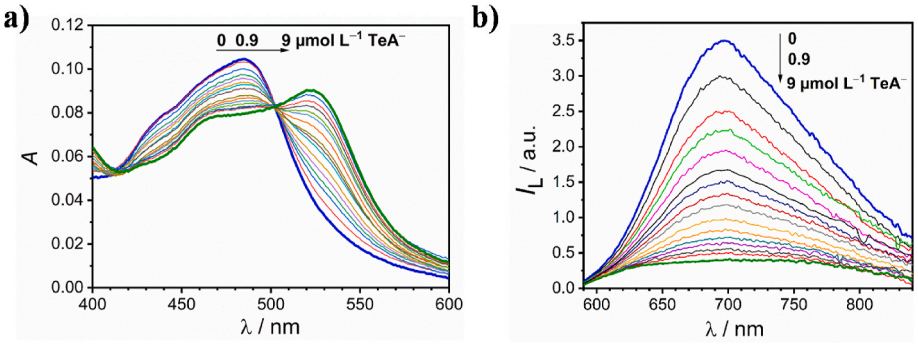

Fig. 1. Changes in the UV–Vis absorption (a) and emission (b) spectra (λ_{exc} = 500 nm) of $[Ru(dab)_2(bim)]^{2+}$ (9.0 x 10^{-6} mol L^{-1}) in acetonitrile upon addition of increasing amounts of the TeA^- anion (as TBA salt).

3.3. Preparation and characterization of the luminescent core-shell SiO_2@Ru-MIP nanoparticles

The procedure to prepare the MIP core-shell nanoparticles doped with the $[Ru(dab)_2(bim)]^{2+}$ luminophore is summarized in Fig. 2. Monodisperse silica nanobeads of ca. 200 nm synthesized by the Stöber method [37] were used as the core material. Then, a MIP nanolayer was grown over the activated silica surface. To obtain a thin homogeneous MIP shell, growth of the latter on the spherical SiO_2 particles was performed by reversible addition-fragmentation chain-transfer (RAFT) polymerization [43]. Firstly, the silica cores were activated with 4-(chloromethyl)phenyltrichlorosilane and then functionalized by nucleophilic substitution with dithiobenzoate to yield a typical RAFT agent [44,45]. The silica-bonded alkyl dithiobenzoate (Fig. 2a) promotes the controlled growth of the MIP around the silica nanobeads by sequential incorporation of monomer units until there are no free monomers left in the medium. RAFT polymerization allows the preparation of polymers with narrow molecular-weight distributions [46].

In this way, the luminescent MIP layer was grown in acetonitrile at 70 °C under an inert atmosphere using a mixture of the synthetic TeA^- (as TBA salt) as template, $[Ru(dab)_2(bim)]^{2+}$ as functional monomer, methacrylamide (MAM) as diluent monomer, and ethylene glycol dimethacrylate (EDMA) as cross-linker, in a 1:1:22:94 mol ratio (Fig. 2a). This is a similar ratio to those employed for growing MIP layers onto silica nanoparticles [31,47]. 2,2′-Azobis(2,4-dimethyl)valeronitrile (ABDV) was used as the low-temperature radical initiator. Non-imprinted polymer (NIP) core-shell nanoparticles were also prepared by following the same procedure but without addition of the template. After 24 h at 70 °C, the resulting MIP/NIP beads were thoroughly washed with a MeOH–TFA (9:1 v/v) mixture to remove the template molecule. Transmission electron microscopy (TEM) images (Fig. 2) confirm the successful growth of a homogenous 10-nm thick MIP layer onto the silica nanoparticles (8 nm in the case of the NIP material). In addition, the presence and homogeneous distribution of Ru in the SiO_2@Ru-MIP (and -NIP) nanoparticles was further confirmed by TEM elemental mapping (Fig. S7).

3.4. Spectroscopic properties of the MIP and NIP nanolayers and their response to TeA

In the first place, the luminescent SiO_2@Ru-MIP nanoparticles to recognize TeA were characterized in acetonitrile for the sake of comparison with the free $[Ru(dab)_2(bim)]^{2+}$ probe. The emission spectrum of the nanoparticles suspended in acetonitrile (Fig. 3) resembles that of the free $[Ru(dab)_2(bim)]^{2+}$ (λ_{em}^{max} = 700 nm), displaying a broader band centered at 695 nm. In the case of the control NIP particles, very similar results are obtained, with their luminescence band peaking at 685 nm.

When increasing amounts of TeA^- (as TBA salt) are added, an important quenching of the luminescent MIP- and NIP-coated silica beads is observed (Fig. 3). This quenching is accompanied by a 35-nm red shift of the emission of the SiO_2@Ru-MIP nanoparticles, but only a 10-nm red shift for the control SiO_2@Ru–NIP. As it has been discussed above for the free dye in solution, these changes suggest hydrogen bonding between the Ru(II)-bim complex and the diketonate molecule also in the polymer matrix. Fig. 3c shows the relative change of the luminescence as a function of the analyte concentration for the MIP and the NIP coatings. In acetonitrile, the TeA-imprinted sites of the MIP nanoparticles do not seem to provide any difference with respect to the unspecific NIP sites. It is important to underline that the sensor response is almost instantaneous: the observed luminescence quenching occurs within just a few seconds after adding TeA^-, showcasing the very fast diffusion of the target molecule through the MIP (or NIP) nanolayer.

Since the final application of the sensing system will probably require the use of some water, we also evaluated the response of the nanobeads to TeA^- in partially aqueous media. In this case, due to the presence of water in the solvent mixture, the use of the tetrabutylammonium tenuazonate was not necessary. The pK_a of TeA is 3.5 [15], so that its anionic form is expected to occur in water. Preparation of water-compatible MIPs whose optical response relies on non-covalent interactions such as electrostatic attraction and hydrogen bonding is challenging. This is particularly relevant if we aim to bind a small molecule such as TeA^-, as water can efficiently compete with the substrate for the binding sites, potentially decreasing the sensitivity and selectivity of the MIP-based chemical sensor [48]. Furthermore, as we discussed above, the optical properties of the luminescent probe are dependent on the water content of the partially organic medium

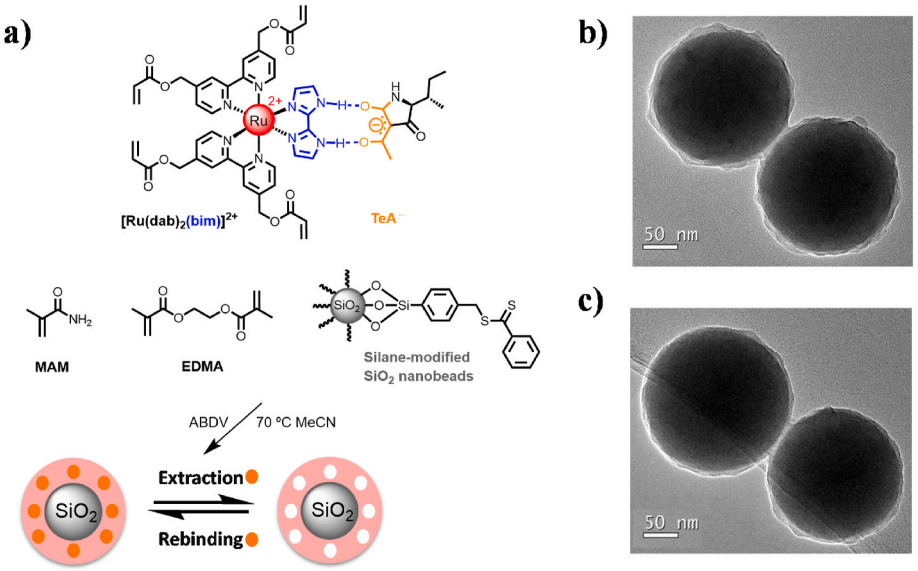

Fig. 2. a) Scheme of the preparation of the luminescent SiO_2@Ru-MIP core-shell nanoparticles for TeA^- recognition (see text). The RAFT polymerization is initiated with ABDV (2,2′-azobis(2,4-dimethyl)valeronitrile) and heat; b) and c) are the TEM images of the obtained MIP and NIP core-shell nanoparticles, respectively. The orange circle represents the tenuazonic acid (TeA) molecules.

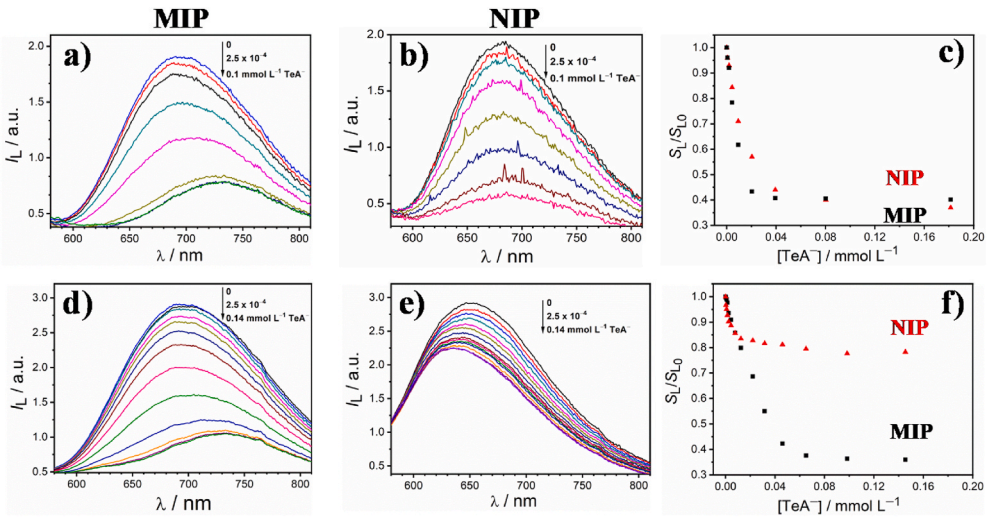

Fig. 3. Changes of the luminescence spectra (λ_{exc} = 500 nm) of 1.12 mg mL^{-1} suspensions of a) SiO_2@Ru-MIP in acetonitrile (MeCN); b) SiO_2@Ru–NIP in MeCN; d) SiO_2@Ru-MIP in MeCN–H_2O (95:5 v/v); e) SiO_2@Ru–NIP in MeCN–H_2O (95:5 v/v), upon addition of increasing amounts of TeA^-. Plots c) and f) depict the area under the emission curve, normalized to the area in the absence of TeA^-, as a function of the TeA^- concentration; black squares for SiO_2@Ru-MIP and red triangles for SiO_2@Ru–NIP in MeCN (c) and MeCN–H_2O (95:5 v/v) (f).

(Figs. S5c–d).

Remarkably enough, addition of 5% water to the acetonitrile suspensions had no substantial effect on the luminescence maximum of the SiO_2@Ru-MIP nanobeads, remaining centered at 695 nm (Fig. 3d). This fact suggests that the polymer backbone is preferentially solvated by the organic solvent. However, the addition of water induces a noticeable blue shift from 685 to 650 nm for the NIP nanoshells (Fig. 3e). As it was discussed above for the free Ru(II) complex in organic solvents, the addition of water leads to significant deprotonation of its biimidazole ligand, resulting in a blue shift of the emission band as the water content increases. The dramatic effect of the presence of 5% water in acetonitrile on the Ru–NIP luminescence points out the very different nature of the TeA binding sites in the imprinted and non-imprinted materials, the latter displaying a higher exposure to the water leading to extensive deprotonation of the coordinated bim ligand.

The TeA dose-response profile of the imprinted luminescent beads is similar in neat acetonitrile and in 5% water−MeCN (Fig. 3c and f); however, the response of the Ru–NIP is much weaker in the presence of water as a result of its loosened interaction with the TeA^- when the probe undergoes deprotonation. The imprinting effect enhancement was also tested with a higher water content (10%, Fig. S8) but, despite the small additional decrease of the non-specific interactions with the NIP, the sensitivity of the MIP system drops significantly. Therefore, a solvent mixture with 5% water in MeCN was chosen for further assays as it provides the best compromise between sensitivity and imprinting effect.

Additionally, since Ru(II) dyes are appreciated for their advantageous long emission lifetimes, we also characterized the sensor system by time-resolved luminescence measurements (Table 1 and Fig. S9). The free $[Ru(dab)_2(bim)]^{2+}$ in aerated acetonitrile requires the sum of two exponentials to successfully fit its luminescence decay. This result suggests that the protonated (short lifetime component) and deprotonated (long lifetime component) forms of the photoexcited dye are contributing, and that there is no fast equilibration between them (otherwise just an exponential decay would be observed [49]). In the case of the Ru-MIP (or NIP) nanolayers, the microheterogeneity around the Ru(II) luminescent probe caused by the polymer scaffold leads to a more complex multi-exponential decay; in that case, a third component with a longer emission lifetime has to be added for a good multi-exponential fit of the excited state decay profile for both the MIP and NIP materials.

For the sake of comparison between the luminescence kinetics of $[Ru(dab)_2(bim)]^{2+}$ in different solvents and within the polymers, we calculated the so-called "pre-exponentially weighted" average lifetime (τ_m; see Table 1 for its definition) of each decay profile. Similar values of τ_m were obtained for the free $[Ru(dab)_2(bim)]^{2+}$ dye and for the luminescent NIP beads in neat MeCN (141 ns and 147 ns, respectively, Table 1) pointing out to a similar solvation of the probe. A comparable situation occurs upon addition of 5% water (209 ns and 240 ns, respectively), being the increase of the excited state lifetime in agreement with the observed emission blue shift (see above) and the energy-gap rule. However, a significantly shorter τ_m occurs when the Ru(II) indicator is covalently tethered to the MIP (141 ns in neat MeCN *vs*. 102 ns for the MIP in the same solvent). A further lowering is observed when 5% water is added to the organic solvent (209 ns *vs*. 72 ns). These results are a consequence of the notably less polar microenvironment around the Ru(II) luminophore when intimately attached to the MIP backbone within its analyte-templated cavities. The decrease of the luminescence lifetime of Ru polypyridyls in going from highly polar organic solvents and water to non-polar media has been documented [50,51]. Interestingly, the probe emission lifetime shows again that the NIP does not

Table 1
Luminescence lifetimes of photoexcited $[Ru(dab)_2(bim)]^{2+}$, SiO_2@Ru-MIP and SiO_2@Ru–NIP core-shell nanoparticles at (25 ± 1 °C) in air-equilibrated media.[a)].

Luminophore	Solvent (v/v)	τ_1/ns (B_1)	τ_2/ns (B_2)	τ_3/ns (B_3)	τ_m/ns[b)]
$[Ru(dab)_2(bim)]^{2+}$	MeCN (100)	93 (19923)	248 (8827)	–	141
$[Ru(dab)_2(bim)]^{2+}$	MeCN + TFA	95 (26339)	259 (5689)	–	124
$[Ru(dab)_2(bim)]^{2+}$	MeCN–H_2O (95:5)	81 (5453)	253 (13943)	–	209
Ru-MIP	MeCN (100)	36 (5543)	126 (6173)	393 (754)	102
Ru-MIP	MeCN–H_2O (95:5)	20 (6673)	110 (2746)	650 (426)	72
Ru–NIP	MeCN (100)	55 (5893)	195 (5531)	582 (651)	147
Ru–NIP	MeCN–H_2O (95:5)	76 (3004)	283 (4220)	645 (768)	240

[a] The luminescence decays are fitted to the equation $I_L = B_0 + \sum_i B_i \tau_i$, being i the number of required exponentials to achieve a $\chi^2 \leq 1.2$.

[b] Pre-exponentially weighted average luminescence lifetime: $\tau_m = \sum_i B_i \tau_i / \sum_i B_i$; estimated uncertainties of the individual lifetimes: bi-exponential fit, ± 2%; tri-exponential fit, ± 3%; of, ±1.5%.

provide the same degree of protection from solvation by water molecules than the MIP (Table 1), pointing out major differences between the structure of the MIP and NIP binding sites.

Regarding the luminescence lifetimes, the most remarkable aspect of the sensor material we have prepared is probably the fact that TeA induces changes in τ_m that can be correlated with its concentration (Fig. 4a and b). To the best of our knowledge, the use of emission lifetime variations to monitor the levels of a target analyte has never been reported for a MIP-based luminescent sensor. Actually, accounts of a fluorescent MIP for cAMP recognition describing emission decays [52,53] did not measure any analyte-related lifetime change. Luminescence lifetime measurements are independent of common disturbances such as light source intensity fluctuations, dye leaching or photobleaching, detector ageing, and interference of the light scattering from the indicator layer. Therefore, lifetime-based sensing is a much more robust analytical method than those relying on luminescence intensity changes, except when ratiometric measurements are used [32].

Fig. 4a shows the τ_m values of the Ru-MIP and Ru–NIP nanoparticles upon addition of TeA^- in MeCN–H_2O (95:5 v/v). These measurements differentiate between specific and non-specific polymer-analyte interactions more clearly than the emission intensity values (Fig. 3f). The presence of TeA^- does not induce any significant change of the τ_m of the SiO_2@Ru–NIP beads (245 ± 5 ns), while a 30% decrease of the average emission lifetime (from 61 ns to 43 ns) is observed for the MIP. Fig. 4b depicts the TeA^- dose-response plot in the 0.50–400 μmol L^{-1} range for the SiO_2@Ru-MIP nanobeads, demonstrating the wider concentration range of the luminescence lifetime-based analytical measurements (compare to those in Fig. 3f). The dose-response curve in the low concentration range was fitted to a 3-parameter rational function [54], and a 382 nmol L^{-1} limit of detection (LOD) was calculated thereof as three times the standard deviation of the blank measurements [55].

3.5. Analytical performance of the SiO_2@Ru-MIP luminescent sensing nanomaterial

Due to the high cost of the mycotoxin, up to this stage we carried out all titration experiments with the home-made TeA that contains ca. 80% of the natural toxin (see Experimental Section). However, to demonstrate the performance of the novel MIP-based TeA-sensitive nanomaterial, we also carried out measurements with the natural toxin. It is worth mentioning that TeA is most often sold as the Cu(II) bis-chelate complex due to the isolation procedure and its intrinsic instability in free form. Obviously, the copper complex cannot be used for our sensing purposes. Therefore, we have isolated natural TeA from the commercial $(TeA)_2Cu$ complex after dissolution in methylene chloride and subsequent elution through a strong cation exchange column [9].

To perform the sensor calibration, the luminescent SiO_2@Ru-MIP nanobeads were suspended in MeCN–H_2O (95:5 v/v) and exposed to increasing concentrations of natural TeA in the 0–0.44 mmol L^{-1} range (Fig. 4c and d). The sample luminescence was recorded immediately after mixing and shaking the cell for a few seconds (longer contact times did not change the results). The same experiments were carried out with the control Ru–NIP beads. The area under the luminescence spectrum against the TeA concentration (Fig. 4d) was fitted to a 3-parameter rational function in the low concentration range [54], and a 324 nmol L^{-1} LOD was calculated thereof as three times the standard deviation of the blank measurements [55]. The reproducibility of the sensor response was evaluated by measuring three calibration curves for each one of the different batches of the SiO_2@Ru-MIP beads (Fig. S10). No significant differences were observed between the dose-response plots, demonstrating the robustness of the photonic sensing material.

The potential cross-reactivity of the sensing system was evaluated in the presence of other mycotoxins that may also be present in food commodities as a consequence of fungi contamination. In this regard, cyclopiazonic acid (CPA), alternariol (AOH) and β-zeranol (β-ZOL), all of which contain a β-hydroxyenone moiety like that of TeA (Fig. 5a), were tested as potential interferents. The selectivity of the TeA-targeted Ru-MIP is demonstrated from the weaker response to those other mycotoxins (Figs. 5b and S11): while natural TeA provoked up to a 35% quenching of the MIP emission, the tested related mycotoxins only caused less than a 10% signal change. The remarkably poor response towards CPA, the molecule with the closest characteristic structure (tetramic acid) to that of TeA, suggests the important contribution of the size selectivity in the target recognition process by the MIP. The same

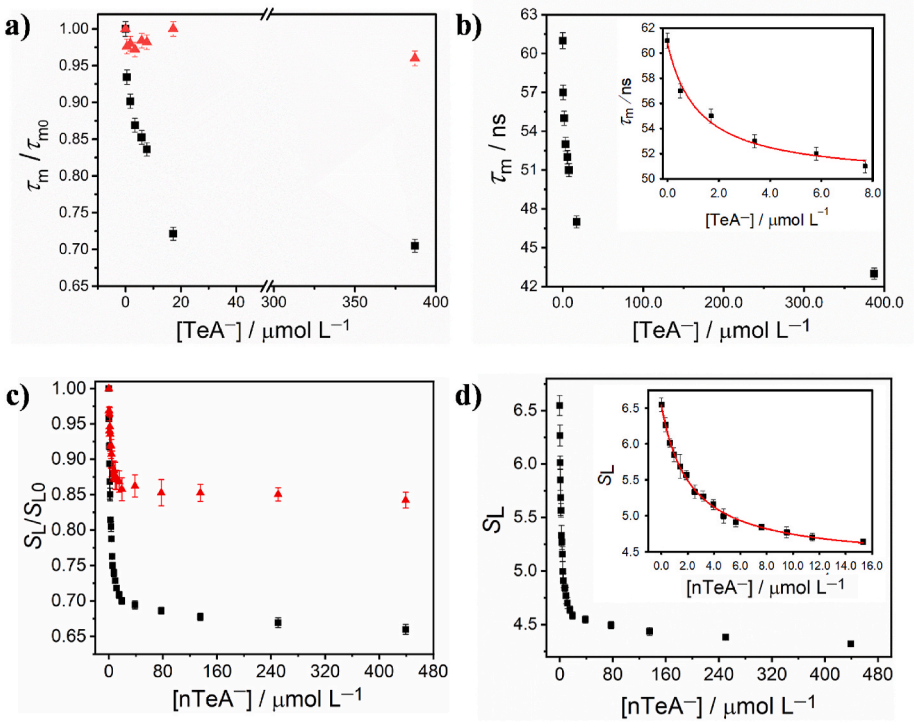

Fig. 4. a) Luminescence lifetimes of SiO_2@Ru-MIP (black squares) and SiO_2@Ru–NIP (red triangles) (λ_{exc} = 463 nm) upon addition of TeA^- in MeCN–H_2O (95:5 v/v) (1.12 mg mL^{-1} of nanoparticles in both cases); the numerical values are collected in Tables S1 and S2 b) TeA^- dose-response plot (n = 3) of the luminescent SiO_2@Ru-MIP particles. The red curve in the zoom inset is the best fit in this concentration range to a three-parameter rational function $f(x) = \frac{(a+bx)}{(1+cx)}$, being the best fit ($r^2$ = 0.993) defined by the following parameters: a = (60.8 ± 0.6), b = (4 ± 1) x 10^4 L μmol^{-1} and c = (8 ± 2) x 10^2 L μmol^{-1}. c) Changes of the luminescence intensity (λ_{exc} = 500 nm; S_L is the area under the emission band) upon addition of natural TeA (nTeA) to a suspension of SiO_2@Ru-MIP (black squares) or SiO_2@Ru–NIP (red triangles) nanoparticles in MeCN–H_2O (95:5 v/v) (1.12 mg mL^{-1} of nanoparticles in both cases). d) nTeA dose-response plot (n = 3) of the luminescent SiO_2@Ru-MIP particles. The red curve in the zoom inset is the best fit in this concentration range to a three-parameter rational function $f(x) = \frac{(a+bx)}{(1+cx)}$, being the best fit ($r^2$ = 0.998) defined by the following parameters: a = (6.54 ± 0.02), b = (2.0 ± 0.1) L μmol^{-1} and c = (0.46 ± 0.03) L μmol^{-1}.

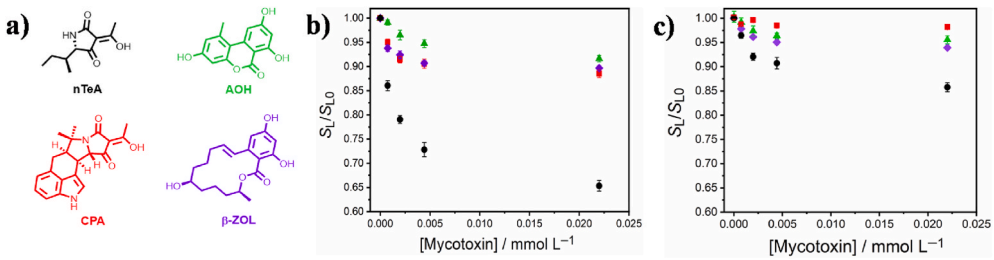

Fig. 5. a) Chemical structure of the mycotoxins tested for cross-sensitivity (tenuazonic acid, cyclopiazonic acid, alternariol and β-zeranol) and variations of the area under the luminescence spectrum of SiO_2@Ru-MIP (b) and SiO_2@Ru–NIP (c) (1.12 mg mL^{-1}) suspended in MeCN–H_2O (95:5 v/v), in the presence of increasing amounts of each mycotoxin (nTeA, black circles; CPA, red squares; AOH, green triangles; β-ZOL, purple spades) (n = 3).

assay performed with the non-imprinted core-shell nanoparticles (Fig. 5c) shows the residual non-specific interactions in the MeCN–H_2O (95:5 v/v) solvent mixture.

The difference between the maximum quenching of the Ru-MIP luminescence attained with the natural TeA (35%, Fig. 5b) and the 65% quenching (Fig. 3f) reached with the synthetic TeA demonstrates the exquisite recognition of the TeA molecule by the novel MIP material. Since the synthetic TeA that has been used as template for the Ru-MIP synthesis is an 81:19 mixture of the natural TeA and its diastereomeric 5*R* epimer (see Materials and Methods section), part of the recognition sites where the Ru indicator dwells remain empty in the presence of the natural TeA leading to lesser quenching of the luminescent material.

A number of optical sensors for TeA detection have been reported (Table S3). However, only one MIP has been described for this purpose. Even without a thorough analytical optimization (not the aim of this study), our TeA-sensitive material improves by an order of magnitude the detectability of that MIP-based luminescent sensor. Other reported sensors are based on immunoassays. In spite of their low LODs, immunosensors require the use of expensive fragile antibodies, diminishing their attractiveness.

4. Conclusions

Thanks to a novel MIP made of a trifunctional acrylate monomer that contains a luminescent Ru(II) complex with a biimidazole ligand in its coordination sphere, tenuazonic acid can be sensed with extraordinary selectivity and speed. Even in partially aqueous medium, the biimidazole moiety forms probably a double hydrogen-bonded adduct with the β-diketonate anionic form of the ionized TeA. Such interaction provides selectivity on top of that imparted by the molecular imprinting effect of the polymer material. Thanks to this feature, closely related toxins such as cyclopiazonic acid are barely recognized. A very fast response to the presence of TeA, achieved by the growth of the luminescent MIP nanoshell onto a 200-nm silica core, would allow real-time sensing of the mycotoxin. The novel optical sensor system can detect down to 63.8 and 75.2 μg L^{-1} of TeA by steady-state and time-resolved luminescence measurements, respectively, for utmost versatility and robustness of the measurements. We expect our first-of-type work will provide the basis for further MIP-based sensors that capitalize on luminescence lifetime rather that absolute emission determinations to free them from instrumental factors that affect the latter. Further work is in progress to exploit the powerful analytical applications of the novel nanomaterials.

CRediT authorship contribution statement

José Quílez-Alburquerque: Data curation, Formal analysis, Investigation, Methodology, Validation, Visualization, Writing – original draft. **Ana B. Descalzo:** Conceptualization, Data curation, Formal analysis, Investigation, Methodology, Supervision, Validation, Visualization. **María C. Moreno-Bondi:** Conceptualization, Funding acquisition, Investigation, Methodology, Project administration, Resources, Supervision, Writing – review & editing. **Guillermo Orellana:** Conceptualization, Funding acquisition, Investigation, Methodology, Project administration, Resources, Supervision, Writing – review & editing.

Declaration of competing interest

The authors declare that they have no known competing financial interests or personal relationships that could have appeared to influence the work reported in this paper.

Acknowledgment

This work was funded by the Spanish Ministry of Science and Innovation (grants CTQ2015-69278-C2-2-R and RTI2018-096410-B-C22/21). J. Q.-A. thanks the Ministry for an F.P.I. doctoral grant.

Appendix A. Supplementary data

Supplementary data to this article can be found online at https://doi.org/10.1016/j.polymer.2021.124041.

References

[1] A. Kumari, N.N. Tirkey (Eds.), Recent Trends in Human and Animal Mycology, Springer Nature, Singapore, 2019.
[2] S. Goyal, K.G. Ramawat, J.M. Mérillon (Eds.), Fungal Metabolites, Springer, Switzerland, 2017.
[3] E. Pfeiffer, N.H. Schebb, J. Podlech, M. Metzler, Novel oxidative in vitro metabolites of the mycotoxins alternariol and alternariol methyl ether, Mol. Nutr. Food Res. 51 (2007) 307–316.
[4] S. Hickert, I. Krug, B. Cramer, H.U. Humpf, Detection and quantitative analysis of the non-cytotoxic allo-tenuazonic acid in tomato products by stable isotope dilution HPLC-MS/MS, J. Agric. Food Chem. 63 (2015) 10879–10884.
[5] H.B. Lee, A. Patriarca, N. Magan, Alternaria in food: ecophysiology, mycotoxin production and toxicology, MYCOBIOLOGY 43 (2015) 93–106.
[6] C. Mujahid, M.C. Savoy, Q. Baslé, P.M. Woo, E.C.Y. Ee, P. Mottier, T. Bessaire, Levels of Alternaria toxins in selected food commodities including green coffe, Toxins 12 (2020) 1–17.
[7] D. Arcella, M. Eskola, J.A. Gómez Ruiz, Dietary exposure assessment to Alternaria toxins in the European population, EFSA J 14 (2016) 4654–4686.
[8] Y. Man, G. Liang, A. Li, L. Pan, Analytical methods for the determination of Alternaria mycotoxins, Chromatographia 80 (2017) 9–22.
[9] D. Siegel, T. Rasenko, M. Koch, I. Nehls, Determination of the Alternaria mycotoxin tenuazonic acid in cereals by high-performance liquid chromatography-electrospray ionization ion-trap multistage mass spectrometry after derivatization with 2,4-dinitrophenylhydrazine, J. Chromatogr. A 1216 (2009) 4582–4588.
[10] T. Zwickel, H. Klaffke, K. Richards, M. Rychlik, Development of a high performance liquid chromatography tandem mass spectrometry based analysis for the simultaneous quantification of various Alternaria toxins in wine, vegetable juices and fruit juices, J. Chromatogr. A 1455 (2016) 74–85.
[11] A.K. Rausch, R. Brockmeyer, T. Schwerdtle, Development and validation of a QuEChERS-based liquid chromatography tandem mass spectrometry multi-method for the determination of 38 native and modified mycotoxins in cereals, J. Agric. Food Chem. 68 (2020) 4657–4669.
[12] L. N Prodi, M. Montalti, Zaccheroni (Eds.), Luminescence Applied in Sensor Science, Springer, Germany, 2011.
[13] B. Pedras (Ed.), Fluorescence in Industry, Springer Nature, Switzerland, 2019.
[14] G. Orellana, D. García-Fresnadillo, in: R. Narayanaswamy, O.S. Wolfbeis (Eds.), Optical Sensors: Industrial, Environmental and Diagnostic Applications, Springer, Germany, 2004, p. 309.

[15] H. Mikula, E. Horkel, P. Hans, C. Hametner, J. Fröhlich, Structure and tautomerism of tenuazonic acid - a synergetic computational and spectroscopic approach, J. Hazard Mater. 250–251 (2013) 308–317.

[16] L. Chen, S.N. Berry, X. Wu, E.N.W. Howe, P.A. Gale, Advances in Anion Receptor Chemistry, Chem 6 (2020) 61–141.

[17] S.A. Rommel, D. Sorsche, M. Fleischmann, S. Rau, Optical sensing of anions via supramolecular recognition with biimidazole complexes, Chem. Eur J. 23 (2017) 18101–18119.

[18] Á.R. Romero Bernal, C.M. Reynoso, V.A. García Londoño, L.E. Broggi, S.L. Resnik, Alternaria toxins in Argentinean wheat, bran, and flour, Food Addit. Contam. Part B Surveill. 12 (2019) 24–30.

[19] J. Zdunek, E. Benito-Peña, A. Linares, A. Falcimaigne-Cordin, G. Orellana, K. Haupt, M.C. Moreno-Bondi, Surface-imprinted nanofilaments for europium-amplified luminescent detection of fluoroquinolone antibiotics, Chem. Eur J. 19 (2013) 10209–10216.

[20] C. Santezi, B.D. Reina, L.N. Dovigo, Curcumin-mediated Photodynamic Therapy for the treatment of oral infections—a review, Photodiagnosis Photodyn. Ther. 21 (2018) 409–415.

[21] G. Ertürk, B. Mattiasson, Molecular imprinting techniques used for the preparation of biosensors, Sensors 17 (2017) 288–305.

[22] J.J. Belbruno, Molecularly imprinted polymers, Chem. Rev. 119 (2019) 94–119.

[23] L. Chen, X. Wang, W. Lu, X. Wu, J. Li, Molecular imprinting: perspectives and applications, Chem. Soc. Rev. 45 (2016) 2137–2211.

[24] R. Gui, H. Jin, Recent advances in synthetic methods and applications of photo-luminescent molecularly imprinted polymers, J. Photochem. Photobiol., A C 41 (2019) 100315–100353.

[25] N.Y. Limaee, S. Rouhani, M.E. Olya, F. Najafi, Selective 2,4-dichlorophenoxyacetic acid optosensor employing a polyethersulfone nanofiber-coated fluorescent molecularly imprinted polymer, Polymer 177 (2019) 73–83.

[26] T. Kajisa, T. Sakata, Molecularly imprinted artificial biointerface for an enzyme-free glucose transistor, ACS Appl. Mater. Interfaces 10 (2018) 34983–34990.

[27] A. Rico-Yuste, J. Walravens, J.L. Urraca, R.A.G. Abou-Hany, A.B. Descalzo, G. Orellana, M. Rychlik, S. De Saeger, M.C. Moreno-Bondi, Analysis of alternariol and alternariol monomethyl ether in foodstuffs by molecularly imprinted solid-phase extraction and ultra-high-performance liquid chromatography tandem mass spectrometry, Food Chem. 243 (2018) 357–364.

[28] A.B. Descalzo, C. Somoza, M.C. Moreno-Bondi, G. Orellana, Luminescent core-shell imprinted nanoparticles engineered for targeted förster resonance energy transfer-based sensing, Anal. Chem. 85 (2013) 5316–5320.

[29] H. Zhang, Molecularly imprinted nanoparticles for biomedical applications, Adv. Mater. 32 (2020) 1806328–1806351.

[30] D. Refaat, M.G. Aggour, A.A. Farghali, R. Mahajan, J.G. Wiklander, I.A. Nicholls, S. A. Piletsky, Strategies for molecular imprinting and the evolution of MIP nanoparticles as plastic antibodies—synthesis and applications, Int. J. Mol. Sci. 20 (2019) 6304–6325.

[31] S. Wagner, J. Bell, M. Biyikal, K. Gawlitza, K. Rurack, Integrating fluorescent molecularly imprinted polymer (MIP) sensor particles with a modular microfluidic platform for nanomolar small-molecule detection directly in aqueous samples, Biosens. Bioelectron. 99 (2018) 244–250.

[32] I. Urriza-Arsuaga, G. Ielasi, M. Bedoya, G. Orellana, in: B. Pedras (Ed.), Fluorescence in Industry, Springer Nature, Switzerland, 2019, p. 1.

[33] J.C. Xiao, J.M. Shreeve, Synthesis of 2,2-biimidazolium-based ionic liquids: use as a new reaction medium and ligand for palladium-catalyzed suzuki cross-coupling reactions, J. Org. Chem. 70 (2005) 3072–3078.

[34] E. Puodziukynaite, J.L. Oberst, A.L. Dyer, J.R. Reynolds, Establishing dual electrogenerated chemiluminescence and multicolor electrochromism in functional ionic transition-metal complexes, J. Am. Chem. Soc. 134 (2012) 968–978.

[35] E.C. Johnson, B.P. Sullivan, D.J. Salmon, S.A. Adeyemi, T.J. Meyer, Synthesis and properties of the chloro-bridged dimer $[(bpy)_2\ RuCl]_2^{2+}$ and its transient 3+ mixed-valence ion, Inorg. Chem. 17 (1978) 2211–2215.

[36] A. Rico-Yuste, R. Abouhany, J.L. Urraca, A.B. Descalzo, G. Orellana, M.C. Moreno-Bondi, Eu(III)-Templated molecularly imprinted polymer used as a luminescent sensor for the determination of tenuazonic acid mycotoxin in food samples, Sensor. Actuator. B Chem. 329 (2021) 129256–129268.

[37] W. Stöber, A. Fink, E. Bohn, Controlled growth of monodisperse silica spheres in the micron size range, J. Colloid Interface Sci. 26 (1968) 62–69.

[38] H.J. Mo, Y.L. Niu, M. Zhang, Z.P. Qiao, B.H. Ye, Photophysical, electrochemical and anion sensing properties of Ru(II) bipyridine complexes with 2,2′-biimidazole-like ligand, Dalton Trans. 40 (2011) 8218–8225.

[39] H.J. Mo, H.Y. Chao, B.H. Ye, A ruthenium biimidazole-like anion receptor with two chelating N-H···O intramolecular hydrogen bonds, Inorg. Chem. Commun. 35 (2013) 100–103.

[40] Y. Cui, H.J. Mo, J.C. Chen, Y.L. Niu, Y.R. Zhong, K.C. Zheng, B.H. Ye, Anion-selective interaction and colorimeter by an optical metalloreceptor based on ruthenium(II) 2,2-biimidazole: hydrogen bonding and proton transfer, Inorg. Chem. 46 (2007) 6427–6436.

[41] P. Gans, A. Sabatini, A. Vacca, Investigation of equilibria in solution. Determination of equilibrium constants with the HYPERQUAD suite of programs, Talanta 43 (1996) 1739–1753.

[42] G. Ielasi, G. Alcover, J. Casellas, C. de Graaf, G. Orellana, M. Reguero, Computer-aided design of short-lived phosphorescent Ru(II) polarity probes, Dyes Pigments 162 (2019) 168–176.

[43] S. Carrasco, E. Benito-Peña, F. Navarro-Villoslada, J. Langer, M.N. Sanz-Ortiz, J. Reguera, L.M. Liz-Marzán, M.C. Moreno-Bondi, Multibranched gold-mesoporous silica nanoparticles coated with a molecularly imprinted polymer for label-free antibiotic surface-enhanced Raman scattering analysis, Chem. Mater. 28 (2016) 7947–7954.

[44] G. Moad, A critical survey of dithiocarbamate reversible addition-fragmentation chain transfer (RAFT) agents in radical polymerization, J. Polym. Sci. Part A Polym. Chem. 57 (2019) 216–227.

[45] S. Beyazit, B. Tse Sum Bui, K. Haupt, C. Gonzato, Molecularly imprinted polymer nanomaterials and nanocomposites by controlled/living radical polymerization, Prog. Polym. Sci. 62 (2016) 1–21.

[46] G. Moad, RAFT polymerization to form stimuli-responsive polymers, Polym. Chem. 8 (2017) 177–219.

[47] S. Wagner, C. Zapata, W. Wan, K. Gawlitza, M. Weber, K. Rurack, On the role of counterions in molecularly imprinted polymers for anionic species, Langmuir 34 (2018) 6963–6975.

[48] W. Wan, A.B. Descalzo, S. Shinde, H. Weißhoff, G. Orellana, B. Sellergren, K. Rurack, Ratiometric fluorescence detection of phosphorylated amino acids through excited-state proton transfer by using molecularly imprinted polymer (MIP) recognition nanolayers, Chem. Eur J. 23 (2017) 15974–15983.

[49] L. Tormo, N. Bustamante, G. Colmenarejo, G. Orellana, Can luminescent Ru(II) Polypyridyl dyes measure pH directly? Anal. Chem. 82 (2010) 5195–5204.

[50] Y. Sun, C. Turro, Highly Solvent Dependent Luminescence from $[Ru(bpy)_n(dppp2)_{3-n}]^{2+}$ (n = 0−2), Inorg. Chem. 49 (2010) 5025–5032.

[51] A.M. Castro, J. Delgado, G. Orellana, Hydrocarbon in water sensing with PTFE membranes doped with a luminescent Ru(II) poly(pyridyl) complex, J. Mater. Chem. 15 (2005) 2952–2958.

[52] B. Wandelt, A. Mielniczak, P. Turkewitsch, S. Wysocki, Steady-state and time-resolved fluorescence studies of fluorescent imprinted polymers, J. Lumin. 102–103 (2003) 774–781.

[53] B. Wandelt, P. Turkewitsch, S. Wysocki, G.D. Darling, Fluorescent molecularly imprinted polymer studied by time-resolved fluorescence spectroscopy, Polymer 43 (2002) 2777–2785.

[54] P.L. Urban, Please avoid plotting analytical response against logarithm of concentration, Anal. Chem. 92 (2020) 10210–10212.

[55] E. Massarini, P. Wästerby, L. Landström, C. Lejon, O. Beck, P.O. Andersson, Methodologies for assessment of limit of detection and limit of identification using surface-enhanced Raman spectroscopy, Sensor. Actuator. B Chem. 207 (2015) 437–446.